Power Dissipation and Magnetic Forces on MAGLEV Rebars

Markus Zahn, *Fellow, IEEE*

***Abstract*—Concrete guideways for proposed MAGLEV vehicles may be reinforced with electrically conducting and magnetizable steel rebars. Transient magnetic fields due to passing MAGLEV vehicles will then induce transient currents in the rebars leading to power dissipation and temperature rise as well as Lorentz and magnetization forces on the rebars. In order to evaluate if this heating and force on the rebars affects concrete life and performance, analysis is presented for an infinitely long conducting and magnetizable cylinder in imposed uniform axial or transverse magnetic fields. Exact and approximate solutions are presented for sinusoidal steady state and step transient magnetic fields inside and outside the cylinder, the induced current density, the vector potential for transverse magnetic fields, the time average dissipated power in the sinusoidal steady state, and the total energy dissipated for step transients. Forces are approximately calculated for imposed magnetic fields with a weak spatial gradient. The analysis is applied to representative rebar materials.**

***Index Terms*—Eddy currents, MAGLEV, magnetic fields, magnetic forces, rebars.**

I. Background

CONCRETE guideways for proposed MAGLEV vehicles may be typically reinforced with steel rebars which are electrically conducting and magnetizable. In the presence of transient magnetic fields due to passing MAGLEV vehicles, transient currents will be induced in the rebars leading to electrical power dissipation and local temperature rise. The induced currents in the presence of a time-varying magnetic field will also cause a transient Lorentz force on the rebar in the direction of weaker magnetic field and thus in the direction away from the vehicle. If the rebar is magnetizable, there is also a magnetization force in the direction of stronger magnetic field and thus in the direction toward the vehicle. The relative strength of these opposing forces are time varying and depend on the magnetic permeability of the rebar, the skin depth, the magnetic diffusion time, the magnetic-field gradient, and the bar radius. The heating and transverse force make it necessary to study if the concrete strength is maintained over the usual life in the presence of time-varying magnetic fields. In order to develop engineering guidelines, the rebar magnetic problem is idealized by considering an infinitely long cylinder with constant ohmic conductivity and constant magnetic permeability with the imposed magnetic field having at most a weak gradient, so that the magnetic-field distribution can be taken as if the imposed field was uniform. The gradient field analysis is necessary to calculate the force on the rebar due to field gradients. In a purely uniform magnetic field, there is no net force on the rebar due either to the Lorentz force on the induced currents or to magnetization. The analysis separately considers the imposed magnetic field to be purely axial or purely transverse to the cylinder axis as shown in Fig. 1. The analysis separately considers the sinusoidal steady state, applicable when many sinusoidal cycles occur, and to step time transients. The analysis is specifically applied to the representative rebar materials listed in Table I.

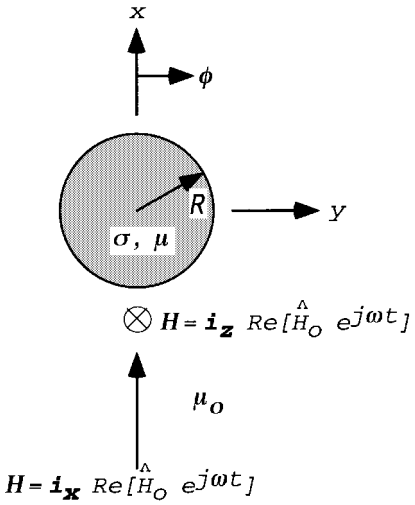

Fig. 1. A cylinder of radius R, ohmic conductivity σ, and magnetic permeability μ is placed in a uniform magnetic field that is either parallel ($H_o\vec{i}_z$) or transverse ($H_o\vec{i}_x$) to the z directed cylinder axis and varies sinusoidally with time at angular frequency ω.

II. Governing Magnetoquasistatic Equations

A. Maxwell's Equations

Maxwell's field equations in the magnetoquasistatic limit for a material with constant magnetic permeability μ and constant ohmic conductivity σ are [1, p. 437]

$$\nabla \times \vec{E} = -\mu \frac{\partial \vec{H}}{\partial t} \quad \text{(Faraday's Law)} \tag{1}$$

$$\nabla \times \vec{H} = \vec{J} = \sigma \vec{E} \quad \text{(Ampere's Law with Ohmic Conduction)} \tag{2}$$

$$\nabla \cdot (\mu \vec{H}) = 0 \quad \text{(Gauss's Law).} \tag{3}$$

Manuscript received January 29, 1996. This work was supported by the U.S. Department of Transportation, National MAGLEV Initiative.

The author is with the Department of Electrical Engineering and Computer Science, Laboratory for Electromagnetic and Electronic Systems, Massachusetts Institute of Technology, Cambridge, MA 02139 USA.

Publisher Item Identifier S 0018-9464(97)00676-6.

TABLE I
ELECTRICAL PROPERTIES, REPRESENTATIVE SKIN-DEPTH $\delta = \sqrt{2/(\omega\mu\sigma)}$ AT 60 Hz, AND REPRESENTATIVE MAGNETIC DIFFUSION TIME $\tau = \sigma\mu R^2$ WITH $R = 1$ cm OF VARIOUS METALS AT 20°C

Material	μ/μ_o	σ (Siemens/m)	δ at 60 Hz (mm)	τ with R = 1 cm
Copper	1	5.80×10^7	8.5	7.3 ns
Aluminum	1	3.53×10^7	10.9	4.4 ns
Steel: mild	5000	8.47×10^6	0.316	5.3 μs
stainless	1	1.10×10^6	62.0	0.14 ns
13 Mn	1.01	1.41×10^6	54.5	0.18 ns
Grade 50 Rebar	3800	4.46×10^6	0.499	2.1 μs
Grade 60 Rebar	3800	4.35×10^6	0.505	2.1 μs

These can be combined into diffusion equations for the magnetic field $\vec{H}$ or the current density $\vec{J}$

$$\nabla^2\vec{H} = \mu\sigma\frac{\partial\vec{H}}{\partial t} \tag{4}$$

$$\nabla^2\vec{J} = \mu\sigma\frac{\partial\vec{J}}{\partial t}. \tag{5}$$

B. Boundary Conditions

Boundary conditions at interfaces of dissimilar materials are the continuity of tangential $\vec{H}$

$$\vec{n}\times[\vec{H}_1 - \vec{H}_2] = 0 \tag{6}$$

and continuity of normal $\vec{B} = \mu\vec{H}$

$$\vec{n}\cdot[\mu_1\vec{H}_1 - \mu_2\vec{H}_2] = 0. \tag{7}$$

C. Dissipated Power

The instantaneous power dissipated per unit axial length, P, in the lossy cylinder of radius R is

$$P = \int_{r=0}^{R}\int_{\phi=0}^{2\pi}\frac{|\vec{J}|^2}{\sigma}rdrd\phi. \tag{8}$$

D. Force Per Unit Axial Length

1) Lorentz Force: The magnetic force per unit axial length on the cylinder due to the Lorentz force on the induced currents in the magnetic field is

$$\vec{f_L} = \int_{r=0}^{R}\int_{\phi=0}^{2\pi}\vec{J}\times\mu\vec{H}rdrd\phi. \tag{9}$$

2) Magnetization Force: The magnetization force on linear magnetizable material with magnetic permeability that depends on space is

$$\begin{aligned}\vec{f_M} &= -\frac{1}{2}\int_{r=0}^{R}\int_{\phi=0}^{2\pi}|\vec{H}|^2\nabla\mu(\vec{r})rdrd\phi \\ &= -\frac{1}{2}\int_{r=0}^{R}\int_{\phi=0}^{2\pi}\left\{\left[H_\phi^2 + H_z^2\right]\nabla\mu(\vec{r})\right. \\ &\qquad \left. - B_r^2\nabla\left(\frac{1}{\mu(\vec{r})}\right)\right\}rdrd\phi.\end{aligned} \tag{10}$$

We separately write terms of tangential $\vec{H}$ and normal $\vec{B}$ at the cylindrical interface at $r = R$ because in the problems to be treated here, the magnetic permeability is uniform within a cylinder and within the surrounding free space. The magnetic permeability varies with position only as a step when crossing the $r = R$ interface where the tangential components of $\vec{H}$, H_ϕ, and H_z are continuous, while the normal component of $\vec{B}$, B_r, is continuous. Since the magnetic permeability is constant everywhere except at the $r = R$ interface where $\mu(\vec{r})$ and $\frac{1}{\mu(\vec{r})}$ take steps, we have that

$$\begin{aligned}\nabla\mu(\vec{r}) &= (\mu_o - \mu)\delta(r-R)\vec{i}_r \\ &= (\mu_o - \mu)\delta(r-R)[\vec{i}_x\cos\phi + \vec{i}_y\sin\phi]\end{aligned} \tag{11}$$

$$\begin{aligned}\nabla\left(\frac{1}{\mu(\vec{r})}\right) &= \left(\frac{1}{\mu_o} - \frac{1}{\mu}\right)\delta(r-R)\vec{i}_r \\ &= \left(\frac{1}{\mu_o} - \frac{1}{\mu}\right)\delta(r-R)[\vec{i}_x\cos\phi + \vec{i}_y\sin\phi].\end{aligned} \tag{12}$$

The spatial impulse at $r = R$, $\delta(r-R)$, indicates that the magnetization force is a surface force. With H_ϕ, H_z, and B_r continuous through the interface, (10) reduces to

$$\begin{aligned}\vec{f_M} = \frac{R}{2}\int_{\phi=0}^{2\pi}&\left[(\mu-\mu_o)\left[H_\phi^2(r=R) + H_z^2(r=R)\right]\right. \\ &\left. + B_r^2(r=R)\left(\frac{1}{\mu_o} - \frac{1}{\mu}\right)\right] \\ &\times[\vec{i}_x\cos\phi + \vec{i}_y\sin\phi]d\phi\end{aligned} \tag{13}$$

where it was convenient to replace the radial unit vector $\vec{i}_r$ by its Cartesian components to explicitly show the ϕ dependence of $\vec{i}_r$. If $|\vec{H}(r=R)|^2$ is an even power trigonometric function of ϕ, the integration of (13) is zero. This will be the case if the applied magnetic field, whether axial or transverse, is uniform. To approximate a realistic magnetic field configuration with a slight nonuniformity over the cylinder, we take the applied magnetic field to be of the form

$$\vec{H} = \vec{H}_o[1 + a\sin\phi] \tag{14}$$

where a is a measure of the magnetic-field gradient. The magnetic field is $(1+a)\vec{H}_o$ at $\phi = \pi/2$ and is $(1-a)\vec{H}_o$ at $\phi = -\pi/2$. With a positive, the field is bigger for positive y than for negative y. If $|a| \ll 1$, the magnetic field and current density solutions are approximately correct if the imposed uniform field is replaced by (14). For our numerical case studies we take $a = 0.1$, corresponding to a maximum of $\pm10\%$ magnetic-field variation at the left and right hand

cylinder edges compared to the top and bottom of the cylinder at $\phi = 0, \pi$ in Fig. 1.

III. Axial Magnetic Field in the Sinusoidal Steady State

A. Exact Solutions for Magnetic Field and Current Density

With an applied uniform axial magnetic field in the z direction varying sinusoidally in time with angular frequency ω, as shown in Fig. 1, the total magnetic field within the cylinder remains purely z directed and is of the form

$$\vec{H}(r,t) = \Re\{\hat{H}_z(r)e^{j\omega t}\}\vec{i}_z. \tag{15}$$

The diffusion equation of (4) then becomes

$$\frac{1}{r}\frac{d}{dr}\left(r\frac{d\hat{H}_z}{dr}\right) = j\omega\mu\sigma\hat{H}_z \quad (0 < r < R). \tag{16}$$

Defining the skin depth as

$$\delta = \sqrt{\frac{2}{\omega\mu\sigma}} \tag{17}$$

(16) is Bessel's equation [2, Sec. 4.8–4.10], [3]

$$r^2\frac{d^2\hat{H}_z}{dr^2} + r\frac{d\hat{H}_z}{dr} - \frac{2jr^2}{\delta^2}\hat{H}_z = 0 \tag{18}$$

with solutions that satisfy the boundary condition

$$\hat{H}_z(r = R) = \hat{H}_o \tag{19}$$

as

$$\hat{H}_z(r) = \frac{\hat{H}_o J_o[(1-j)r/\delta]}{J_o[(1-j)R/\delta]}. \tag{20}$$

The current density is obtained from Ampere's law as

$$\vec{J} = \nabla \times \vec{H} \Rightarrow \hat{J}_\phi(r) = -\frac{d\hat{H}_z}{dr} = \frac{\hat{H}_o(1-j)}{\delta}\frac{J_1[(1-j)r/\delta]}{J_o[(1-j)R/\delta]}. \tag{21}$$

B. Exact Solution for Dissipated Power Per Unit Length

The time average power dissipation per unit length after integrating over ϕ in (8) is then

$$\begin{aligned}\langle P\rangle &= \pi\int_{r=0}^{R}\frac{|\hat{J}_\phi|^2}{\sigma}rdr \\ &= \frac{2\pi|\hat{H}_o|^2}{\sigma\delta^2|J_o[(1-j)R/\delta]|^2} \\ &\quad\times\int_{r=0}^{R} J_1[(1-j)r/\delta]J_1[(1+j)r/\delta]rdr.\end{aligned} \tag{22}$$

The last integral is a Lommel integral [3, pp. 102–104], [4, Appendix B], [5, p. 199] which is exactly integrable

$$\begin{aligned}&\int_{r=0}^{R} rJ_n[(1+j)r/\delta]J_n[(1-j)r/\delta]dr \\ &\quad= \frac{R\delta}{2}\Re\{(j-1)J_n[(1-j)R/\delta]J_{n-1}[(1+j)R/\delta]\}.\end{aligned} \tag{23}$$

For our problem $n = 1$ so that (22) reduces to

$$\begin{aligned}\langle P\rangle &= \frac{\pi|\hat{H}_o|^2R}{\sigma\delta|J_0[(1-j)R/\delta]|^2} \\ &\quad\times\Re\{(j-1)J_1[(1-j)R/\delta]J_0[(1+j)R/\delta]\}.\end{aligned} \tag{24}$$

C. Nondimensional Solutions

It is convenient to use dimensionless variables by normalizing all variables to the applied magnetic field amplitude $\hat{H}_o$ and to the cylinder radius R

$$\begin{aligned}&\tilde{H}_z(\tilde{r}) = \frac{\hat{H}_z(r)}{\hat{H}_o},\ \tilde{J}_\phi(\tilde{r}) = \hat{J}_\phi(r)R/\hat{H}_o,\ \tilde{r} = r/R,\ \tilde{\delta} = \delta/R; \\ &\langle\tilde{P}\rangle = \frac{\langle P\rangle\sigma}{\pi|\hat{H}_o|^2}\end{aligned} \tag{25}$$

so that the solutions of (20) and (21) are

$$\tilde{H}_z(\tilde{r}) = \frac{\hat{H}_z}{\hat{H}_o} = \frac{J_o[(1-j)\tilde{r}/\tilde{\delta}]}{J_o[(1-j)/\tilde{\delta}]} \tag{26}$$

$$\tilde{J}_\phi(\tilde{r}) = \frac{\hat{J}_\phi(r)R}{\hat{H}_o} = \frac{(1-j)}{\tilde{\delta}}\frac{J_1[(1-j)\tilde{r}/\tilde{\delta}]}{J_o[(1-j)/\tilde{\delta}]}. \tag{27}$$

For $\tilde{\delta} > 1$ the magnetic field is fairly uniform over the cylinder cross section, and the current density is approximately linear with radius with peak amplitude at $\tilde{r} = 1$. As $\tilde{\delta}$ becomes much less than unity, the magnetic field and current density decrease exponentially from $\tilde{r} = 1$ with penetration depth about equal to $\tilde{\delta}$. As $\tilde{\delta}$ becomes small, the current density becomes very large at $\tilde{r} = 1$ approaching a surface current as $\tilde{\delta} \to 0$.

The nondimensional power per unit length from (24) is

$$\begin{aligned}\langle\tilde{P}\rangle &= \frac{\langle P\rangle\sigma}{\pi|\hat{H}_o|^2} \\ &= \int_0^1 |\tilde{J}_\phi|^2\tilde{r}d\tilde{r} \\ &= \frac{\Re\{[(j-1)J_1[(1-j)/\tilde{\delta}]J_o[(1+j)/\tilde{\delta}]\}}{\tilde{\delta}|J_o[(1-j)/\tilde{\delta}]|^2}.\end{aligned} \tag{28}$$

Fig. 2 plots the nondimensional dissipated power per unit length in (28) versus nondimensional skin depth, $\tilde{\delta} = \delta/R$. Fig. 3 applies (24) to the materials in Table I and plots dimensional dissipated power per unit length versus frequency f in hertz, $f = \omega/2\pi$, for a representative cylinder radius of $R = 1.0$ cm with an applied peak magnetic field strength of $|\mu_o\hat{H}_o| = 0.5$ T.

D. Force Per Unit Length

1) Lorentz Force Per Unit Length: In a perfectly uniform applied field, the Lorentz force of (9) would integrate to zero. We thus assume that the applied magnetic field has the slight nonuniformity over the cylinder given by (14). The Lorentz volume force density [N·m^3] is

$$\vec{F}_L = \vec{J}\times\mu\vec{H} = \mu J_\phi H_z\vec{i}_r = \mu J_\phi H_z[\cos\phi\vec{i}_x + \sin\phi\vec{i}_y] \tag{29}$$

where we convert to Cartesian coordinates to explicitly show the ϕ dependence of $\vec{i}_r$. Substituting (29) into (9) gives the time

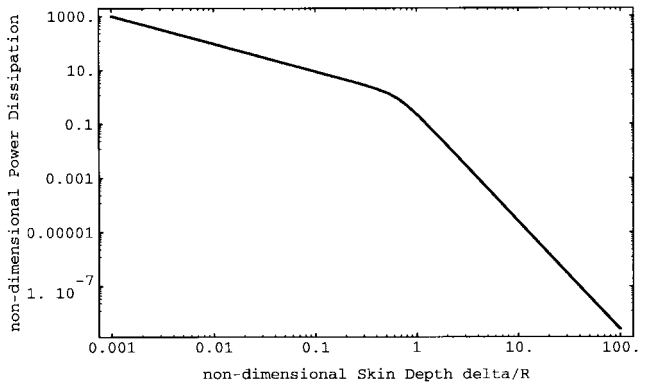

Fig. 2. Nondimensional dissipated power of (28), $\langle \bar{P} \rangle = \langle P \rangle \sigma / [\pi |\hat{H}_o|^2]$, versus nondimensional skin depth, $\bar{\delta} = \delta / R$, in a lossy magnetizable cylinder placed in a uniform axial magnetic field.

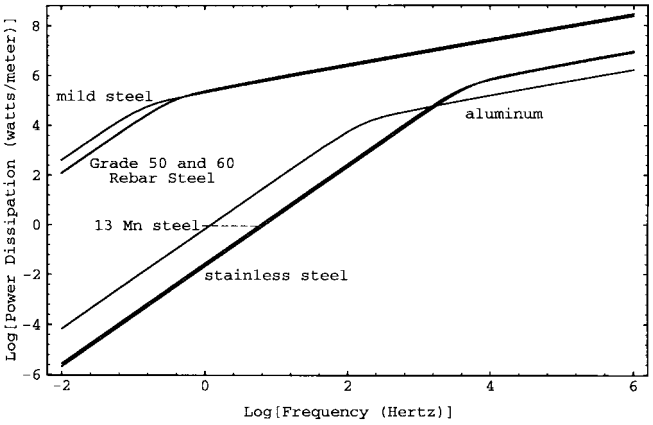

Fig. 3. Dimensional dissipated power per unit length (W/m) of (24) for an axial magnetic field versus frequency in hertz for materials in Table I for representative radius $R = 1.0$ cm with peak magnetic field strength $|\mu_o \hat{H}_o| = 0.5$ T.

average Lorentz force per unit length as purely $-y$ directed ($\langle f_{Lx} \rangle = 0$), in the direction of weak magnetic field

$$\begin{aligned}\langle f_{Ly} \rangle &= \frac{1}{2} \Re \left\{ \int_{r=0}^{R} \int_{\phi=0}^{2\pi} \mu \hat{J}_\phi \hat{H}_z^* \sin\phi r dr d\phi \right\} \\ &= \frac{\mu |\hat{H}_o|^2}{2\delta |J_o[(1-j)]R/\delta]|^2} \\ &\quad \times \Re \left\{ (1-j) \int_{r=0}^{R} \int_{\phi=0}^{2\pi} \sin\phi [1 + a \sin\phi]^2 \right. \\ &\qquad \left. \times J_o[(1+j)r/\delta] J_1[(1-j)r/\delta] r dr d\phi \right\} \\ &= \frac{\pi a \mu |\hat{H}_o|^2}{\delta |J_o[(1-j)R/\delta]|^2} \\ &\quad \times \Re \left\{ \int_{r=0}^{R} (1-j) J_1[(1-j)r/\delta] J_o[(1+j)r/\delta] r dr \right\}. \end{aligned} \tag{30}$$

It is also convenient to nondimensionalize all forces per unit length as

$$\langle \tilde{f} \rangle = \frac{\langle f \rangle}{\pi a \mu R |\hat{H}_o|^2} \tag{31}$$

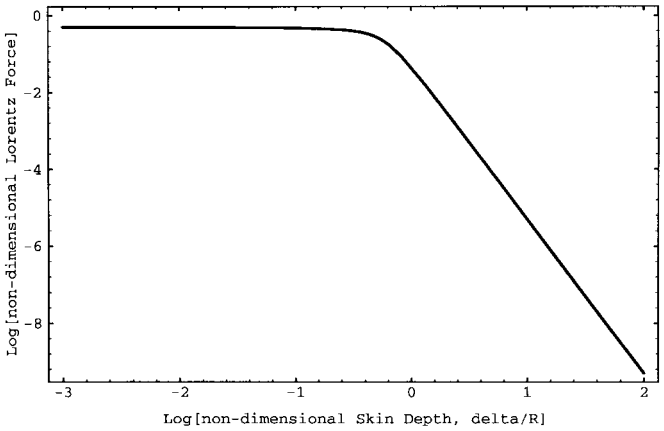

Fig. 4. Magnitude of nondimensional $-y$ directed Lorentz force per unit length of (32), $\langle \bar{f}_{Ly} \rangle = \langle f_{Ly} \rangle / [\pi a \mu R |\hat{H}_o|^2]$, versus nondimensional skin depth, $\bar{\delta} = \delta / R$, of a lossy magnetizable cylinder placed in a uniform axial magnetic field.

so that (30) becomes

$$\begin{aligned}\langle \tilde{f}_{Ly} \rangle &= \frac{\langle f_{Ly} \rangle}{\pi a \mu R |\hat{H}_o|^2} = \frac{1}{\tilde{\delta} |J_o[(1-j)/\tilde{\delta}]|^2} \\ &\quad \times \Re \left\{ (1-j) \int_0^1 J_1[(1-j)\tilde{r}/\tilde{\delta}] J_o[(1+j)\tilde{r}/\tilde{\delta}] \tilde{r} d\tilde{r} \right\}. \end{aligned} \tag{32}$$

The integration over $\tilde{r}$ is done numerically and gives the nondimensional plot in Fig. 4.

E. Magnetization Force Per Unit Length

The time average of the magnetization force in (13) with the weak gradient magnetic field of (14) is

$$\begin{aligned}\langle \vec{f}_M \rangle &= \frac{1}{4} (\mu - \mu_o) |\hat{H}_o|^2 R \\ &\quad \times \int_{\phi=0}^{2\pi} [1 + a \sin\phi]^2 [\vec{i}_x \cos\phi + \vec{i}_y \sin\phi] d\phi \end{aligned} \tag{33}$$

which has $\langle f_{Mx} \rangle = 0$ and

$$\langle f_{My} \rangle = \frac{1}{2} (\mu - \mu_o) |\hat{H}_o|^2 \pi a R. \tag{34}$$

Fig. 5 plots the magnitude of the dimensional y component of the total time average force per unit axial length, $\langle f_y \rangle = \langle f_{Ly} \rangle + \langle f_{My} \rangle$, versus frequency for materials in Table I taking R to be 1.0 cm, $a = 0.1$, and $|\mu_o \hat{H}_o| = 0.5$ T. Note that for nonmagnetic materials and for magnetic steel materials at high frequency when the Lorentz force dominates, the force is always $-y$ directed, that is, in the direction of decreasing magnetic field. For magnetic steel materials, the force is $+y$ directed at low frequencies due to the cylinder magnetization being attracted to strong magnetic field regions. The dips in the force curves of magnetizable steels show the force passing through zero as it reverses sign on the log-log plots.

F. Approximate Limits

It is clear from the breakpoints in dissipated power and force plots of Figs. 2–5 that the solutions have approximate

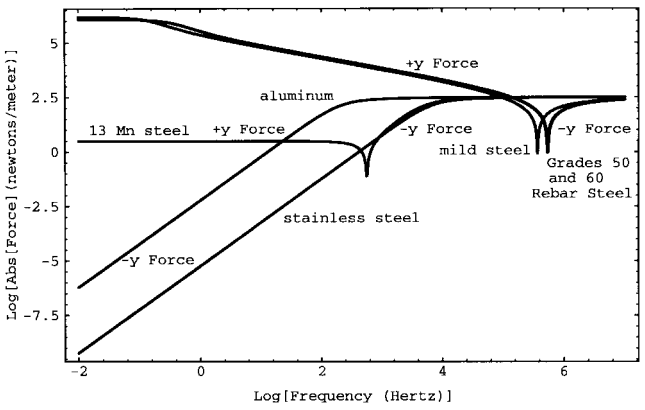

Fig. 5. Magnitude of the total dimensional force per unit length (N/m) in the y direction versus frequency in hertz due to the sum of Lorentz and magnetization forces of (30) and (34) from an axial magnetic field with a weak gradient, $a = 0.1$, in the y direction given by (14) for representative radius $R = 1.0$ cm with peak magnetic field strength of $|\mu_o \hat{H}_o| = 0.5$ T.

limiting expressions for skin depth large or small compared to cylinder radius.

1) Small Skin Depth Limit, $\delta/R \ll 1$: When $\delta/R \ll 1$, the zero and first order Bessel functions approximately reduce to [2, Sec. 4.9]

$$J_o[(1-j)r/\delta] \approx \sqrt{\frac{\delta(1-j)}{\pi r}}\frac{e^{(1+j)r/\delta}}{2}$$
$$J_1[(1-j)r/\delta] \approx -j\sqrt{\frac{\delta(1-j)}{\pi r}}\frac{e^{(1+j)r/\delta}}{2}. \quad (35)$$

Then the dimensional and nondimensional magnetic field and current density distributions approximately reduce to

$$\hat{H}_z(r) \approx \hat{H}_o\sqrt{\frac{R}{r}}e^{(1+j)(r-R)/\delta}$$
$$\tilde{H}_z(\tilde{r}) \approx \frac{\hat{H}_z(r)}{\hat{H}_o} = \frac{1}{\sqrt{\tilde{r}}}e^{(1+j)(\tilde{r}-1)/\tilde{\delta}}$$
$$\hat{J}_\phi(r) \approx -\frac{\hat{H}_o(1+j)}{\delta}\sqrt{\frac{R}{r}}e^{(1+j)(r-R)/\delta}$$
$$\tilde{J}_\phi(\tilde{r}) \approx \frac{\hat{J}_\phi(r)R}{\hat{H}_o} = -\frac{(1+j)}{\tilde{\delta}\sqrt{\tilde{r}}}e^{(1+j)(\tilde{r}-1)/\tilde{\delta}}. \quad (36)$$

The dimensional and nondimensional time average dissipated power per unit length and time average total force per unit length in the weak gradient magnetic field of (14) are then

$$\langle P\rangle \approx \frac{\pi R|\hat{H}_o|^2}{\sigma\delta}$$
$$\langle\tilde{P}\rangle = \frac{\langle P\rangle\sigma}{\pi|\hat{H}_o|^2} \approx \frac{1}{\tilde{\delta}} \quad (37)$$
$$\langle f_y\rangle \approx -\frac{\mu_o\pi aR}{2}|\hat{H}_o|^2$$
$$\langle\tilde{f}_y\rangle = \frac{\langle f_y\rangle}{\pi a\mu R|\hat{H}_o|^2} \approx -\frac{\mu_o}{2\mu}. \quad (38)$$

To approximately verify (37) we realize that for small skin depth, all the current is approximately confined to a skin depth thick layer at the $r = R$ surface. With the magnetic field at $r = R$ equal to $\hat{H}_o$ dropping to approximately zero within the small distance δ from the interface, the effective surface current density, which equals the discontinuity in tangential $\hat{H}$ at the interface, is $\hat{K}_\phi \approx -\hat{H}_o$. Then the volume current density magnitude within this skin depth thick layer is $|\hat{J}_\phi| \approx |\hat{K}_\phi/\delta| \approx |\hat{H}_o|/\delta$. The time average power dissipated per unit length is then approximately

$$\lim_{\delta/R\ll 1}\langle P\rangle \approx \frac{1}{2}\frac{|\hat{J}_\phi|^2}{\sigma}2\pi R\delta \approx \frac{|\hat{H}_o|^2\pi R}{\sigma\delta} \quad (39)$$

in agreement with (37).

Similarly, (38) can be verified by approximately computing the Lorentz force on the surface current in the weak gradient magnetic field of (14)

$$\lim_{\delta/R\ll 1}\langle\vec{f}_L\rangle$$
$$\approx \frac{1}{4}\Re\int_{\phi=0}^{2\pi}\vec{K}\times\mu\vec{H}^*Rd\phi$$
$$= \frac{1}{4}\Re\int_{\phi=0}^{2\pi}\mu\hat{K}_\phi\hat{H}_z^*\vec{i}_rRd\phi$$
$$= -\frac{\mu R|\hat{H}_o|^2}{4}\int_{\phi=0}^{2\pi}[1+a\sin\phi]^2[\vec{i}_x\cos\phi+\vec{i}_y\sin\phi]d\phi$$
$$= -\frac{\mu R\pi a|\hat{H}_o|^2}{2}\vec{i}_y. \quad (40)$$

When (40) is added to the magnetization force of (34), the total time average force per unit length agrees with (38).

2) Large Skin Depth Limit, $\delta/R \gg 1$: When $\delta/R \gg 1$, the zero and first order Bessel functions approximately reduce to [2, Sec. 4.8]

$$J_o[(1-j)r/\delta] \approx 1 + \frac{jr^2}{2\delta^2}$$
$$J_1[(1-j)r/\delta] \approx \frac{(1-j)r}{2\delta}\left[1+\frac{jr^2}{4\delta^2}\right]. \quad (41)$$

It is necessary to expand to order $1/\delta^3$ in order to properly calculate the first order force per unit axial length which varies as $1/\delta^4$, as in some cases the higher order terms integrate to zero. The dimensional and nondimensional magnetic field and current density distributions then reduce to

$$\hat{H}_z(r) \approx \hat{H}_o\frac{\left[1+\frac{jr^2}{2\delta^2}\right]}{\left[1+j\frac{R^2}{2\delta^2}\right]}$$
$$\tilde{H}_z(\tilde{r}) = \frac{\hat{H}_z(r)}{\hat{H}_o} \approx \frac{1+\frac{j\tilde{r}^2}{2\tilde{\delta}^2}}{1+\frac{j}{2\tilde{\delta}^2}} \quad (42)$$
$$\hat{J}_\phi(r) \approx -\frac{j\hat{H}_o}{\delta^2}r\left[1-\frac{jR^2}{2\delta^2}\right]\left[1+\frac{jr^2}{4\delta^2}\right]$$
$$\tilde{J}_\phi(\tilde{r}) = \frac{\hat{J}_\phi(r)R}{\hat{H}_o} \approx -\frac{j\tilde{r}}{\tilde{\delta}^2}\left[1-\frac{j}{2\tilde{\delta}^2}\right]\left[1+\frac{j\tilde{r}^2}{4\tilde{\delta}^2}\right]. \quad (43)$$

The approximate dimensional and nondimensional power per unit length and force per unit length in a weak gradient magnetic field are then

$$\langle P\rangle \approx \frac{\pi R^4|\hat{H}_o|^2}{4\sigma\delta^4}$$
$$\langle \tilde{P}\rangle = \frac{\langle P\rangle\sigma}{\pi|\hat{H}_0|^2} \approx \frac{1}{4\tilde{\delta}^4} \tag{44}$$
$$\langle f_y\rangle \approx \left[\frac{1}{2}(\mu-\mu_o) - \frac{\mu R^4}{20\delta^4}\right]\pi aR|\hat{H}_o|^2$$
$$\langle \tilde{f}_y\rangle = \frac{\langle f_y\rangle}{\pi a\mu R|\hat{H}_o|^2} \approx \frac{1}{2}\left(1-\frac{\mu_o}{\mu}\right) - \frac{1}{20\tilde{\delta}^4}. \tag{45}$$

These results can also be checked with a simple approximate model. If the skin depth is much larger than the cylinder radius, the internal magnetic field approximately equals the imposed field, $\hat{H}_z(r) \approx \hat{H}_o$, and the induced magnetic field due to induced eddy currents is small. Applying the integral form of Faraday's Law to a circular contour of radius r approximately gives

$$\oint_C \vec{E}\cdot\vec{dl} = -\frac{d}{dt}\int_S \vec{B}\cdot\vec{da} \Rightarrow E_\phi 2\pi r = -\pi r^2\mu\frac{dH_z}{dt} \tag{46}$$

which can be solved for the induced current density as

$$\hat{J}_\phi(r) = \sigma\hat{E}_\phi(r) = -\frac{\sigma\mu r}{2}j\omega\hat{H}_o = -\frac{jr}{\delta^2}\hat{H}_o \tag{47}$$

which approximately agrees with the predominant term in (43). The time average power dissipated per unit length is then

$$\lim_{\delta/R\gg 1}\langle P\rangle = \frac{1}{2}\int_{r=0}^{R}\frac{|\hat{J}_\phi|^2}{\sigma}2\pi r dr$$
$$= \frac{\pi|\hat{H}_o|^2}{\sigma\delta^4}\int_0^R r^3 dr = \frac{\pi|\hat{H}_o|^2R^4}{4\sigma\delta^4} \tag{48}$$

in agreement with (44). Note that the time average of the Lorentz force density term of (29), $\Re(\hat{J}_\phi\mu\hat{H}_z^*)$, would be zero using (47). This is why higher order terms are needed in (42) and (43).

IV. Transverse Magnetic Field in the Sinusoidal Steady State

A. Exact Solution for Magnetic Field and Current Density

Fig. 1 also shows a uniform transverse magnetic field in the x direction varying sinusoidally in time with angular frequency ω. The resulting magnetic field then has r and ϕ components while the induced current has only a z component. Because the direction of $\vec{H}$ varies with position, the vector Laplacian in cylindrical coordinates in (4) is different and more complicated than the scalar Laplacian. However, with the direction of $\vec{J}$ constant with position the vector Laplacian in (5) equals the simpler scalar Laplacian, so we choose to solve (5) for the

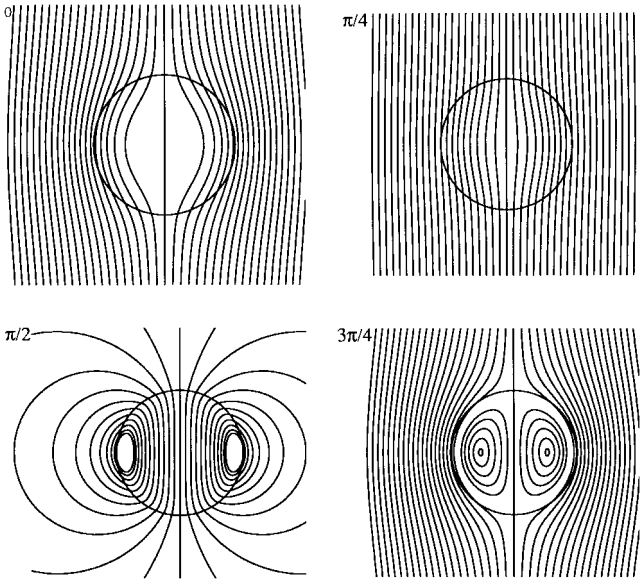

Fig. 6. Magnetic field lines of (58) with $\hat{H}_o$ real at various values of ωt given at upper left during the sinusoidal cycle for $\bar{\delta} = 0.5$ and $\mu/\mu_o = 1$.

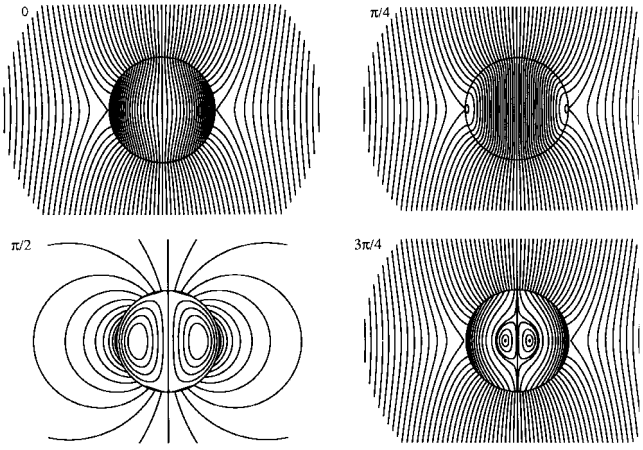

Fig. 7. Magnetic-field lines of (58) with $\hat{H}_o$ real at various values of ωt given at upper left during the sinusoidal cycle for $\bar{\delta} = 0.5$ and $\mu/\mu_o = 3800$.

current density. We take the current density to be of the form

$$J_z(r,\phi,t) = \Re\{\hat{J}_z(r)\sin\phi e^{j\omega t}\} \tag{49}$$

so that (5) becomes

$$\frac{d^2\hat{J}_z}{dr^2} + \frac{1}{r}\frac{d\hat{J}_z}{dr} - \hat{J}_z\left[\frac{1}{r^2}+\frac{2j}{\delta^2}\right] = 0 \tag{50}$$

with solution of the form

$$\hat{J}_z(r) = CJ_1[(1-j)r/\delta] \tag{51}$$

where C is a complex constant to be determined from boundary conditions. The magnetic-field distribution inside the cylinder is found from (51) using Faraday's law of (1)

$$\nabla\times\left(\frac{\vec{J}}{\sigma}\right) = -\mu\frac{d\vec{H}}{dt} \tag{52}$$

while outside the cylinder the magnetic field is the uniform applied field plus a line dipole field due to the induced current

which results from solutions to Laplace's equation for a scalar magnetic potential or a z directed vector potential, as shown in (53) at the bottom of the next page, where C and D are found from the boundary conditions of continuity of tangential $\vec{H}$ and normal $\vec{B}$ at $r = R$

$$H_\phi(r = R_-) = H_\phi(r = R_+);$$
$$B_r(r = R) = \mu H_r(r = R_-) = \mu_o H_r(r = R_+). \quad (54)$$

The general solutions for the constants C and D are shown in (55) and (56), found at the bottom of the page. Note that for $\mu/\mu_o = 1$, C and D greatly simplify, $C = 4\hat{H}_o/[(j+1)\delta J_o[(1-j)R/\delta]]$ and $D = \hat{H}_o R^2[-1 + 2\delta J_1[(1-j)R/\delta]/[(1-j)RJ_o[(1-j)R/\delta]]$.

B. Magnetic-Field Lines

The magnetic-field lines at any instant of time are the lines of constant magnetic vector potential A_z defined as

$$\vec{B} = \nabla \times \vec{A} = \vec{i}_r \frac{1}{r}\frac{\partial A_z}{\partial \phi} - \vec{i}_\phi \frac{\partial A_z}{\partial r}. \quad (57)$$

The vector potential is then obtained from (53) as

$$A_z(r,\phi,t) = \begin{cases} \Re\left\{\frac{j\mu\delta^2 C}{2} J_1[(1-j)r/\delta]\sin\phi e^{j\omega t}\right\}, & 0 < r < R \\ \Re\left\{\mu_o\left[\hat{H}_o r + \frac{D}{r}\right]\sin\phi e^{j\omega t}\right\}, & r > R. \end{cases} \quad (58)$$

Figs. 6–7 take $\hat{H}_o$ to be real and plot the magnetic-field lines at various times during the sinusoidal cycle for $\tilde{\delta} = 0.5$ and values of $\mu/\mu_o = 1$ and $\mu/\mu_o = 3800$ as representative for nonmagnetic and magnetic materials in Table I. Self-magnetic field contributions due to the induced current result in closed magnetic-field lines that do not terminate at $r \to \infty$. This is most easily seen at $\omega t = \pi/2$ when the applied magnetic field is instantaneously zero.

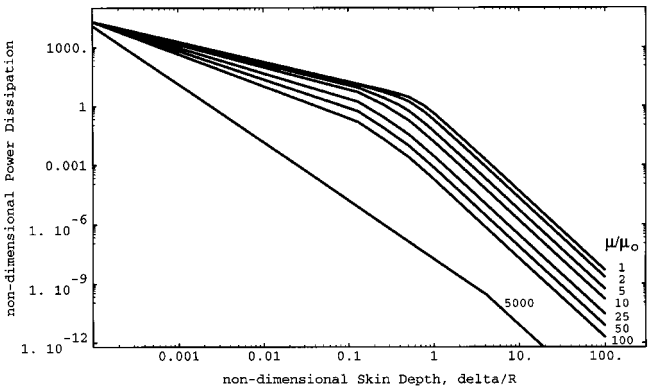

Fig. 8. Nondimensional dissipated power from (59), $\langle \bar{P} \rangle = \langle P \rangle \sigma/\pi|\hat{H}_o|^2$, versus nondimensional skin depth, $\bar{\delta} = \delta/R$, and magnetic permeability in a lossy magnetizable cylinder placed in a uniform transverse magnetic field.

C. Exact Solution for Dissipated Power Per Unit Length

The time average power dissipation per unit length is

$$\langle P \rangle = \frac{\pi}{2}\int_{r=0}^{R} \frac{|\hat{J}_z(r)|^2}{\sigma} r dr$$
$$= \frac{\pi|C|^2}{2\sigma}\int_{r=0}^{R} J_1[(1-j)r/\delta]J_1[(1+j)r/\delta] r dr$$
$$= \frac{\pi|C|^2 R\delta}{4\sigma}\Re\{(j-1)J_1[(1-j)R/\delta]J_o[(1+j)R/\delta]\} \quad (59)$$

where we use the Lommel integral formula of (23) with $n = 1$. Note that for $\mu/\mu_o = 1$, the dissipated power in (59) for a transverse magnetic field is twice that for an axial magnetic field given by (24). Using the nondimensional definitions of (25), Fig. 8 plots (59) versus $\tilde{\delta} = \delta/R$ for various values of μ/μ_o, while Fig. 9 plots the dimensional dissipated power per unit length versus frequency for materials in Table I for representative cylinder radius $R = 1.0$ cm with a peak applied magnetic field strength of $|\mu_o \hat{H}_o| = 0.5$ T.

D. Force Per Unit Length

1) Lorentz Force Per Unit Length: For the Lorentz force density, it is convenient to write cylindrical unit vectors in

$$\hat{\vec{H}}(r,\phi) = \begin{cases} \frac{jC\delta^2}{2}\left[\vec{i}_r \frac{1}{r} J_1[(1-j)r/\delta]\cos\phi - \vec{i}_\phi\left[\frac{(1-j)}{\delta} J_o[(1-j)r/\delta] - \frac{1}{r}J_1[(1-j)r/\delta]\right]\sin\phi\right] & 0 < r < R \\ \left[\hat{H}_o + \frac{D}{r^2}\right]\cos\phi\vec{i}_r - \left[\hat{H}_o - \frac{D}{r^2}\right]\sin\phi\vec{i}_\phi & r > R \end{cases} \quad (53)$$

$$C = \frac{2\mu_o R}{j\mu\delta^2}\frac{[\hat{H}_o + D/R^2]}{J_1[(1-j)R/\delta]} = \frac{4\mu_o R\hat{H}_o}{j\mu\delta^2\left[J_1[(1-j)R/\delta] + \frac{\mu_o}{\mu}\left[\frac{(1-j)R}{\delta}J_o[(1-j)R/\delta] - J_1[(1-j)R/\delta]\right]\right]} \quad (55)$$

$$\frac{D}{R^2} = \hat{H}_o \frac{J_1[(1-j)R/\delta] - \frac{\mu_o}{\mu}\left[\frac{(1-j)R}{\delta}J_o[(1-j)R/\delta] - J_1[(1-j)R/\delta]\right]}{J_1[(1-j)R/\delta] + \frac{\mu_o}{\mu}\left[\frac{(1-j)R}{\delta}J_o[(1-j)R/\delta] - J_1[(1-j)R/\delta]\right]} \quad (56)$$

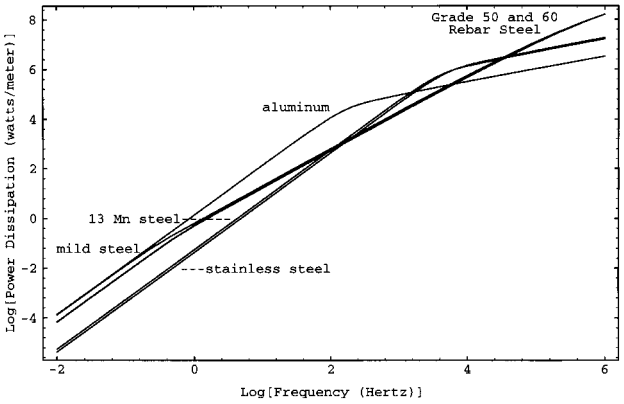

Fig. 9. Dimensional dissipated power per unit length (W/m) of (59) in a transverse magnetic field versus frequency in Hertz for materials in Table I for representative radius $R = 1.0$ cm and peak magnetic field strength $|\mu_o \hat{H}_o| = 0.5$ T.

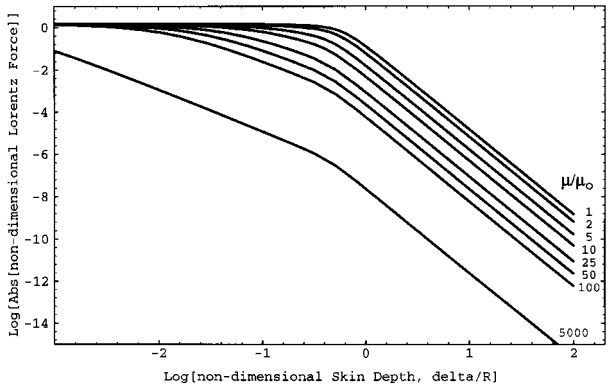

Fig. 10. Magnitude of the nondimensional $-y$ directed Lorentz force per unit length of (61), $\langle \tilde{f}_{Ly} \rangle = \langle f_{Ly} \rangle / [\pi a \mu R |\hat{H}_o|^2]$, versus nondimensional skin depth, $\tilde{\delta} = \delta/R$, for various magnetic permeabilities of a lossy magnetizable cylinder placed in a uniform transverse magnetic field.

terms of Cartesian unit vectors

$$\vec{F}_L = \vec{J} \times \mu \vec{H} = \mu J_z [H_r \vec{i}_\phi - H_\phi \vec{i}_r]$$
$$= \mu J_z [H_r(-\sin\phi \vec{i}_x + \cos\phi \vec{i}_y) - H_\phi(\cos\phi \vec{i}_x + \sin\phi \vec{i}_y)]. \quad (60)$$

The total Lorentz force per unit length is obtained from (9) by integrating (60) over the cylinder cross sectional area. Again using the weak-gradient approximation of (14), the nondimensional time average Lorentz force per unit length becomes after integration over ϕ

$$\langle \tilde{f}_{Ly} \rangle = \frac{\langle f_{Ly} \rangle}{\pi a \mu R |\hat{H}_o|^2}$$
$$= \Re \left\{ \int_{\tilde{r}=0}^{1} \frac{1}{4} \tilde{J}_z^*(\tilde{r}) [\tilde{H}_r(\tilde{r}) - 3\tilde{H}_\phi(\tilde{r})] \tilde{r} d\tilde{r} \right\}. \quad (61)$$

Evaluating by numerical integration for various values of μ/μ_o, we find the Lorentz force is $-y$ directed with a positive and varies with frequency as shown in Fig. 10.

E. Magnetization Force Per Unit Length

The time average magnetization force per unit length is obtained by substituting (53), (55), and (56) into (13) to yield

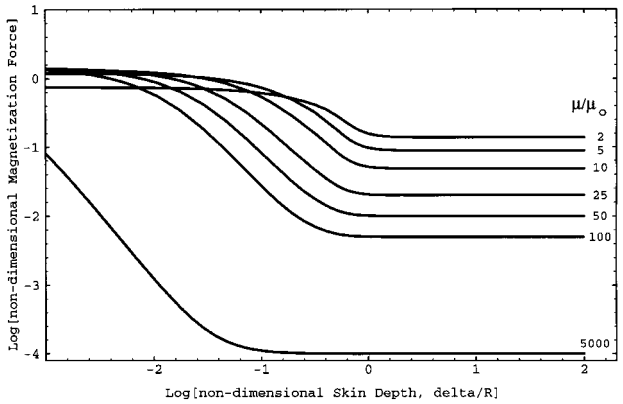

Fig. 11. Magnitude of the nondimensional $+y$ directed magnetization force per unit length of (62), $\langle \tilde{f}_{My} \rangle = \langle f_{My} \rangle / [\pi a \mu R |\hat{H}_o|^2]$, versus nondimensional skin depth, $\tilde{\delta} = \delta/R$, for various magnetic permeabilities of a lossy magnetizable cylinder placed in a uniform transverse magnetic field.

$\langle f_{Mx} \rangle = 0$ and

$$\langle \tilde{f}_{My} \rangle = \frac{\langle f_{My} \rangle}{\pi a \mu R |\hat{H}_o|^2}$$
$$= \frac{1}{8} \left[\frac{3(\mu - \mu_o)}{\mu} |\tilde{H}_\phi(\tilde{r}=1)|^2 + \frac{\mu_o}{\mu} \left(1 - \frac{\mu}{\mu_o}\right) |\tilde{B}_r(\tilde{r}=1)|^2 \right] \quad (62)$$

where $\tilde{B}_r(\tilde{r}=1) = \hat{B}_r(r=R)/\mu_o \hat{H}_o$. This $+y$ directed nondimensional magnetization force is plotted versus δ/R in Fig. 11.

Fig. 12 shows the magnitude of the sum of nondimensional Lorentz and magnetization forces.

The total dimensional magnetic force per unit axial length is plotted versus frequency in Fig. 13 for materials in Table I for representative radius of $R = 1.0$ cm in a peak magnetic field of $|\mu_o \hat{H}_o| = 0.5$ T with weak gradient parameter $a = 0.1$. Note that for the nonmagnetic materials, the total force is due only to the Lorentz force and is $-y$ directed, that is in the direction of decreasing magnetic field, while for the magnetizable steels the force is $+y$ directed at low frequencies where the magnetization force dominates and is $-y$ directed at high frequencies where the Lorentz force dominates.

F. Approximate Limits

We again see breakpoints in the plots of Figs. 8–13.

1) Small Skin Depth Limit, $\delta/R \ll 1$: Using the approximate small skin depth Bessel function approximations in (35), approximate forms for the nondimensional transverse field solutions can be found. However, because some of the Bessel function terms in (55)–(56) are divided by μ/μ_o which can be very large for ferromagnetic materials, it is necessary to expand some terms to higher powers of $\tilde{\delta}$. The effects of large magnetic permeability can be seen in Figs. 8 and 10 where the transition from small to large skin depth limits becomes less sharp as μ/μ_o becomes larger. The approximate solutions

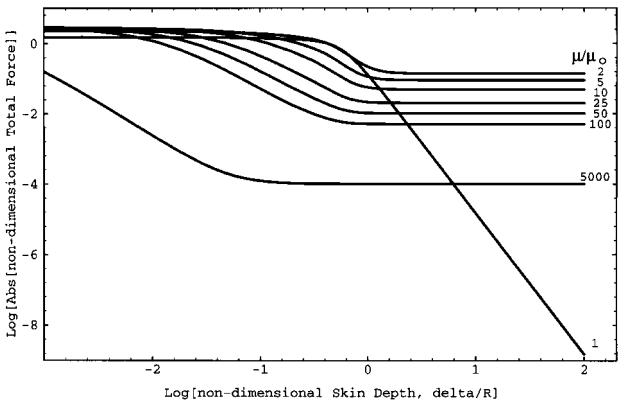

Fig. 12. Magnitude of the sum of nondimensional $-y$ directed Lorentz force per unit length and $+y$ directed magnetization force per unit length, $\langle \tilde{f}_{Ly} \rangle + \langle \tilde{f}_{My} \rangle = \langle f_{Ly} + f_{My} \rangle / [\pi a \mu R |\hat{H}_o|^2]$ of (61) and (62), versus nondimensional skin depth, $\tilde{\delta} = \delta / R$, for various magnetic permeabilities of a lossy magnetizable cylinder placed in a uniform transverse magnetic field.

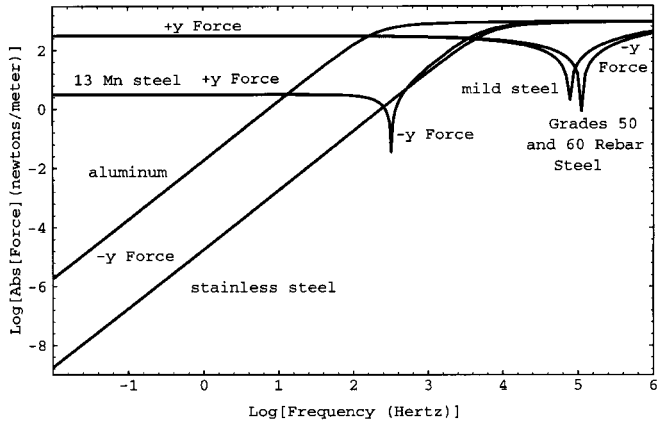

Fig. 13. Magnitude of the total dimensional force per unit length (N/m) in the y direction from (61) and (62) versus frequency in hertz due to the sum of Lorentz and magnetization forces from a transverse magnetic field for materials in Table I with a weak gradient magnetic field in the y direction, $a = 0.1$, for representative radius $R = 1.0$ cm, with peak magnetic field strength of $|\mu_o \hat{H}_o| = 0.5$ T.

are then

$$\tilde{C} = \frac{CR}{\hat{H}_o} \approx \frac{-8j\mu_o e^{-(1+j)/\tilde{\delta}}}{\mu\tilde{\delta}^2\sqrt{(1-j)\tilde{\delta}/\pi}[-j+\mu_o(1-j)/(\mu\tilde{\delta})]}$$

$$\tilde{D} = \frac{D}{\hat{H}_o R^2} \approx -\frac{[j+\mu_o(1-j)/(\mu\tilde{\delta})]}{[-j+\mu_o(1-j)/(\mu\tilde{\delta})]}$$

$$\tilde{\vec{H}}(\tilde{r},\phi) = \frac{\vec{H}(r,\phi)}{\hat{H}_o} \approx -\frac{2\mu_o}{\mu\sqrt{\tilde{r}}}\frac{e^{(1+j)(\tilde{r}-1)/\tilde{\delta}}}{[-j+\mu_o(1-j)/(\mu\tilde{\delta})]} \times \left[\frac{j}{\tilde{r}}\cos\phi\vec{i}_r + \frac{(1-j)}{\tilde{\delta}}\sin\phi\vec{i}_\phi\right] \quad 0<r<R$$

$$\tilde{J}_z(\tilde{r},\phi) = \frac{\hat{J}_z(r,\phi)R}{\hat{H}_o} \approx -\frac{4\mu_o\sin\phi e^{(1+j)(\tilde{r}-1)/\tilde{\delta}}}{\mu\tilde{\delta}^2\sqrt{\tilde{r}}[-j+\mu_o(1-j)/(\mu\tilde{\delta})]} \quad 0<r<R \tag{63}$$

$$\langle\tilde{P}\rangle = \frac{\langle P\rangle\sigma}{\pi|\hat{H}_o|^2} \approx \frac{2}{\tilde{\delta}\left[1+\frac{\mu}{\mu_o}\tilde{\delta}+\frac{1}{2}\left(\frac{\mu}{\mu_o}\right)^2\tilde{\delta}^2\right]}$$

$$\langle\tilde{f}_{Ly}\rangle = \frac{\langle f_{Ly}\rangle}{\pi a\mu R|\hat{H}_o|^2} \approx -\frac{3}{2\left[1+\frac{\mu}{\mu_o}\tilde{\delta}+\frac{1}{2}\left(\frac{\mu}{\mu_o}\right)^2\tilde{\delta}^2\right]}$$

$$\langle\tilde{f}_{My}\rangle = \frac{\langle f_{My}\rangle}{\pi a\mu R|\hat{H}_o|^2} \approx \frac{\frac{(\mu-\mu_o)}{\mu_o}\left[\frac{6\mu_o}{\mu}+\tilde{\delta}^2\right]}{4\left[1+\frac{\mu}{\mu_o}\tilde{\delta}+\frac{1}{2}\left(\frac{\mu}{\mu_o}\right)^2\tilde{\delta}^2\right]}$$

$$\langle\tilde{f}_y\rangle = \langle\tilde{f}_{Ly}\rangle + \langle\tilde{f}_{My}\rangle \approx -\frac{\frac{3\mu_o}{2\mu}-\left(\frac{\mu-\mu_o}{4\mu_o}\right)\tilde{\delta}^2}{\left[1+\frac{\mu}{\mu_o}\tilde{\delta}+\frac{1}{2}\left(\frac{\mu}{\mu_o}\right)^2\tilde{\delta}^2\right]}.$$

We can approximately check these results by realizing that for small skin depth, the magnetic field just outside the cylinder is approximately the same as if the cylinder were perfectly conducting. Then the predominant magnetic field should be tangential

$$\vec{H}(r=R,\phi) \approx -2\hat{H}_o\sin\phi\vec{i}_\phi \tag{64}$$

and the current density is

$$|\hat{J}_z(r=R,\phi)| \approx \left|\frac{\hat{H}_\phi(r=R,\phi)}{\delta}\right| = \frac{2|\hat{H}_o|\sin\phi}{\delta}. \tag{65}$$

The time average dissipated power unit length is then

$$\lim_{\delta/R\ll 1}\langle P\rangle \approx \frac{1}{2}\int_0^{2\pi}\frac{|J_z(r=R,\phi)|^2\delta R d\phi}{\sigma} \approx \frac{2\pi R|\hat{H}_o|^2}{\sigma\delta} \tag{66}$$

in agreement with the dominant power term in (63).

Similarly, the time average Lorentz force per unit length with an effective surface current at $r=R$, $K_z \approx H_\phi$, is

$$\lim_{\delta/R\ll 1}\vec{f}_L \approx \frac{1}{2}\int_{\phi=0}^{2\pi}\vec{K}\times\mu\vec{H}Rd\phi = -\frac{1}{2}\int_{\phi=0}^{2\pi}K_z\mu H_\phi\vec{i}_r Rd\phi = -\frac{\mu R}{2}\int_{\phi=0}^{2\pi}H_\phi^2[\vec{i}_x\cos\phi+\vec{i}_y\sin\phi]d\phi. \tag{67}$$

Then on the time average, using the weak gradient expression of (14) with (64)

$$\lim_{\delta/R\ll 1}\langle\vec{f}_L\rangle \approx -\mu|\hat{H}_o|^2R\int_{\phi=0}^{2\pi}[1+a\sin\phi]^2\sin^2\phi \times[\vec{i}_x\cos\phi+\vec{i}_y\sin\phi]d\phi = -2\mu Ra|\hat{H}_o|^2\vec{i}_y\int_{\phi=0}^{2\pi}\sin^4\phi d\phi = -\frac{3\mu\pi Ra|\hat{H}_o|^2}{2}\vec{i}_y \tag{68}$$

in agreement with the predominant term in (63).

1) Large Skin Depth Limit, $\delta/R \gg 1$: Using the approximate large skin depth relations in (41), the nondimensional transverse field solutions approximately reduce to

$$\tilde{C} = \frac{CR}{\hat{H}_o} \approx -\frac{8j\mu_o}{\tilde{\delta}(1-j)(\mu+\mu_o)}\left[1-\frac{j(3\mu_o+\mu)}{4\tilde{\delta}^2(\mu+\mu_o)}\right]$$

$$\tilde{D} = \frac{D}{\hat{H}_o R^2} \approx \frac{(\mu-\mu_o)}{(\mu+\mu_o)} - \frac{j\mu\mu_o}{\tilde{\delta}^2(\mu+\mu_o)^2}$$

$$\tilde{H}_r(\tilde{r},\phi) = \frac{\hat{H}_r(r,\phi)}{\hat{H}_o} \approx \frac{2\mu_o}{(\mu+\mu_o)}$$

$$\times\left[1+\frac{j}{4\tilde{\delta}^2}\left(\tilde{r}^2-\frac{(3\mu_o+\mu)}{(\mu_o+\mu)}\right)\right]\cos\phi \qquad 0<r<R$$

$$\tilde{H}_\phi(\tilde{r},\phi)=\frac{\hat{H}_\phi(r,\phi)}{\hat{H}_o}\approx-\frac{\mu_o}{(\mu+\mu_o)} \times\left[2+\frac{j}{2\tilde{\delta}^2}\left(3\tilde{r}^2-\frac{(3\mu_o+\mu)}{(\mu_o+\mu)}\right)\right]\sin\phi \qquad 0<r<R$$

$$\tilde{J}_z(\tilde{r},\phi)=\frac{\hat{J}_z(r,\phi)R}{\hat{H}_o}\approx\frac{-2j\mu_o\tilde{r}}{\tilde{\delta}^2(\mu+\mu_o)} \times\left[2+\frac{j}{2\tilde{\delta}^2}\left(\tilde{r}^2-\frac{(3\mu_o+\mu)}{(\mu_o+\mu)}\right)\right]\sin\phi \qquad 0<r<R$$

$$\langle\tilde{P}\rangle=\frac{\langle P\rangle\sigma}{\pi|\hat{H}_o|^2}\approx\frac{2\mu_o^2}{\tilde{\delta}^4(\mu+\mu_o)^2}$$

$$\langle\tilde{f}_{Ly}\rangle=\frac{\langle f_{Ly}\rangle}{\pi a\mu R|\hat{H}_o|^2}\approx-\frac{3\mu_o^2}{5\tilde{\delta}^4(\mu+\mu_o)^2}$$

$$\langle\tilde{f}_{My}\rangle=\frac{\langle f_{My}\rangle}{\pi a\mu R|\hat{H}_o|^2}\approx\frac{(3+\mu/\mu_o)(\mu-\mu_o)\mu_o^2}{2\mu(\mu+\mu_o)^2}. \tag{69}$$

These results can be checked by realizing that when $\delta/R\gg 1$ the predominant magnetic field in the cylinder is $\hat{H}_x=\frac{2\mu_o\hat{H}_o}{(\mu+\mu_o)}$, with negligible contribution from the induced current. Then applying the integral form of Faraday's law to a z directed rectangular contour at r and angles ϕ and $\phi+\pi$ we obtain

$$\hat{J}_z(r,\phi)=\sigma\hat{E}_z(r,\phi)=\frac{-2j\omega\mu\sigma\mu_o r}{\mu+\mu_o}\sin\phi\hat{H}_o =-\frac{4j}{\delta^2}\frac{\mu_o}{\mu+\mu_o}r\sin\phi\hat{H}_o \tag{70}$$

which is the dominant current density term in (69). The time average dissipated power per unit axial length is then

$$\lim_{\delta/R\gg1}\langle P\rangle=\frac{1}{2}\int_{r=0}^{R}\int_{\phi=0}^{2\pi}\frac{|\hat{J}_z(r,\phi)|^2}{\sigma}rdrd\phi =\frac{8\mu_o^2|\hat{H}_o|^2}{\sigma\delta^4(\mu+\mu_o)^2}\int_{r=0}^{R}\int_{\phi=0}^{2\pi}r^3\sin^2\phi drd\phi =\frac{2\pi\mu_o^2R^4|\hat{H}_o|^2}{\sigma\delta^4(\mu+\mu_o)^2} \tag{71}$$

in agreement with the power in (69). Note again that using (70) in the time average y directed Lorentz force density term $\Re(\hat{J}_z\mu\hat{H}_x^*)$ gives zero force. This is why higher order terms in the magnetic field and current density are needed in (69).

V. Step Change in Axial Magnetic Field

A. Turn-On Transient

We now consider an axial magnetic field that is instantaneously stepped on at time $t=0$ to an amplitude H_o. The magnetic field in the cylinder is also axially directed for all time and can be expressed in the form

$$H_z(r,t)=H_o+\hat{H}(r)e^{-\alpha t}\quad(0<r<R) \tag{72}$$

where we recognize that in the steady state, $(t\to\infty)$, the magnetic field in the cylinder approaches the applied magnetic field H_o. The magnetic field diffusion rate α is not yet known. Substituting the assumed form of solution of (72) into the magnetic diffusion equation of (4) gives

$$r^2\frac{d^2\hat{H}}{dr^2}+r\frac{d\hat{H}}{dr}+\alpha\sigma\mu r^2\hat{H}=0 \tag{73}$$

with solution that is finite at $r=0$

$$\hat{H}(r)=AJ_o(\sqrt{\alpha\sigma\mu}r). \tag{74}$$

At $r=R$, the tangential component of $\vec{H}$ must be continuous so that $H_z(r=R,t)=H_o$, which then requires that $\hat{H}(r=R)=0$. This requires that

$$\sqrt{\alpha\sigma\mu}R=\beta_n \tag{75}$$

where β_n is the nth zero of the zeroth order Bessel function, $J_0(\beta_n)=0$, for which the first 20 values are given in the left most column of Table II.

Thus, there are an infinite number of α's, and we can write the most general form of solution as

$$H_z(r,t)=H_o+\sum_{n=1}^{\infty}A_nJ_o(\beta_nr/R)e^{-\alpha_nt} \tag{76}$$

where

$$\alpha_n=\beta_n^2/(\sigma\mu R^2). \tag{77}$$

To find the amplitudes A_n, we use the initial condition at $t=0$ that the magnetic field in the cylinder is zero

$$H_z(r,t=0)=0=H_o+\sum_{n=1}^{\infty}A_nJ_o(\beta_nr/R). \tag{78}$$

Using the orthogonality condition for Bessel functions that [6, p. 485]

$$\int_0^R rJ_o(\beta_mr/R)J_o(\beta_nr/R)dr=\begin{cases}0, & m\neq n\\ \frac{R^2}{2}J_1^2(\beta_m), & m=n\end{cases} \tag{79}$$

we solve (78) for A_n as

$$A_n=\frac{-2H_o}{\beta_nJ_1(\beta_n)} \tag{80}$$

so that the magnetic field and current density are

$$H_z(r,t)=H_o\left[1-2\sum_{n=1}^{\infty}\frac{J_o(\beta_nr/R)}{\beta_nJ_1(\beta_n)}e^{-\beta_n^2t/\tau}\right]$$

$$J_\phi(r,t)=-\frac{\partial H_z}{\partial r}=-\frac{2H_o}{R}\sum_{n=1}^{\infty}\frac{J_1(\beta_nr/R)}{J_1(\beta_n)}e^{-\beta_n^2t/\tau} \tag{81}$$

where $\tau=\sigma\mu R^2$ is a representative magnetic diffusion time. The steady-state uniform magnetic field in the cylinder is approximately reached for $t/\tau>0.5$ as the induced current density becomes small. At early times, $t/\tau<0.1$, the current density is largest near the interface, $r/R=1$, as the initial surface current $K_\phi=-H_z$ at $t=0$, diffuses into the cylinder.

The dissipated power per unit length is then

$$P=\int_0^R\frac{J_\phi^2}{\sigma}2\pi rdr =\frac{8\pi H_o^2}{\sigma R^2}\int_0^R\left[\sum_{n=1}^{\infty}\frac{J_1(\beta_nr/R)}{J_1(\beta_n)}e^{-\beta_n^2t/\tau}\right]^2rdr. \tag{82}$$

TABLE II
ROOTS TO THE MODAL EQUATION FROM (108): $\mu_o\beta_n J_o(\beta_n) + (\mu - \mu_o)J_1(\beta_n) = 0$

n	$\mu/\mu_o = 1$ $[J_0(\beta_n) = 0$, ref.6, p. 409]	$\mu/\mu_o = 1.01$	$\mu/\mu_0 = 10$	$\mu/\mu_0 = 3800$	$\mu/\mu_o = 5000$	$\mu/\mu_o = \infty$ $[J_1(\beta_n) = 0$, ref. 6, p. 409]
1	2.4048	2.4090	3.4798	3.8307	3.8309	3.8317
2	5.5201	5.5219	6.4201	7.0137	7.0142	7.0156
3	8.6537	8.6549	9.3926	10.1708	10.1714	10.1735
4	11.7915	11.7924	12.4054	13.3202	13.3210	13.3237
5	14.9309	14.9316	15.4502	16.4663	16.4673	16.4706
6	18.0711	18.0716	18.5183	19.6107	19.6119	19.6159
7	21.2116	21.2121	21.6030	22.7541	22.7555	22.7601
8	24.3525	24.3529	24.6995	25.8969	25.8985	25.9037
9	27.4935	27.4938	27.8048	29.0392	29.0410	29.0468
10	30.6346	30.6349	30.9166	32.1812	32.1832	32.1897
11	33.7758	33.7761	34.0334	35.3230	35.3252	35.3323
12	36.9171	36.9174	37.1540	38.4646	38.4671	38.4748
13	40.0584	40.0587	40.2777	41.6061	41.6088	41.6171
14	43.1998	43.2000	43.4038	44.7475	44.7504	44.7593
15	46.3412	46.3414	46.5319	47.8889	47.8919	47.9015
16	49.4826	49.4828	49.6616	51.0301	51.0333	51.0435
17	52.6241	52.6242	52.7926	54.1713	54.1747	54.1856
18	55.7655	55.7657	55.9248	57.3124	57.3161	57.3275
19	58.9070	58.9072	59.0580	60.4536	60.4574	60.4695
20	62.0485	62.0486	62.1920	63.5946	63.5986	63.6114

$$\lim_{\beta \gg 1} \beta \approx \tan^{-1}\left[\frac{\mu - \mu_o(1+\beta)}{\mu - \mu_o(1-\beta)}\right]$$

A general Bessel function orthogonality relation that extends (79) is [6, p. 485]

$$\int_0^R rJ_\nu(\beta_m r/R)J_\nu(\beta_n r/R)dr = \begin{cases} 0, & m \neq n, \nu > -1 \\ \frac{R^2}{2}\left[\frac{dJ_\nu(\beta_n)}{d\beta_n}\right]^2, & m = n, b = 0, \nu > -1 \\ \frac{R^2}{2\beta_n^2}\left[\frac{a^2}{b^2} + \beta_n^2 - \nu^2\right]J_\nu^2(\beta_n), & m = n, b \neq 0, \nu > -1 \end{cases} \tag{83}$$

where β_m and β_n are positive zeros of

$$aJ_\nu(x) + bx\frac{dJ_\nu(x)}{dx} = 0 \tag{84}$$

with a and b real constants. Note that (79) is obtained for $\nu = 0$ with $b = 0$. To evaluate (82) we must integrate the square of the infinite series of first order Bessel functions with parameters β_n that are the zeros of the zeroth order Bessel function. Expanding the square of the infinite series in (82) term by term results in integrals like that on the left side of (83) with $\nu = 1$. Recognizing that

$$\frac{dJ_1(x)}{dx} = J_o(x) - \frac{J_1(x)}{x} \tag{85}$$

lets us rewrite (84) with $\nu = 1$ as

$$J_1(x)(a - b) + bxJ_o(x) = 0. \tag{86}$$

If we set $a = b$, then (86) reduces to finding the zeros of the zeroth order Bessel function, which are the β_n in the left-most column of Table II. Thus with $a = b$ and $\nu = 1$, (83) reduces to

$$\int_0^R rJ_1(\beta_m r/R)J_1(\beta_n r/R)dr = \begin{cases} 0, & m \neq n \\ \frac{R^2}{2}J_1^2(\beta_n), & m = n. \end{cases} \tag{87}$$

Applying (87) to (82) gives

$$P = \frac{4\pi H_o^2}{\sigma}\sum_{n=1}^{\infty} e^{-2\beta_n^2 t/\tau} \tag{88}$$

and the total dissipated energy per unit length is

$$W = \int_0^\infty Pdt = 2\pi\mu H_o^2 R^2 \sum_{n=1}^{\infty}\frac{1}{\beta_n^2}. \tag{89}$$

Using the left-most values of β_n in Table II, we obtain $W \approx 2\pi\mu H_o^2 R^2(0.246)$. The magnetization and Lorentz forces per unit length for a slightly nonuniform magnetic field as given by (14) are obtained from (9) and (13) as

$$\begin{aligned} \vec{f}_M &= \frac{1}{2}(\mu - \mu_o)H_0^2 R \\ &\quad \times \int_{\phi=0}^{2\pi}[1 + a\sin\phi]^2[\vec{i}_x\cos\phi + \vec{i}_y\sin\phi]d\phi \\ &= (\mu - \mu_o)H_o^2\pi Ra\vec{i}_y \end{aligned} \tag{90}$$

$$\begin{aligned} \vec{f}_L &= \int_{r=0}^{R}\int_{\phi=0}^{2\pi}\mu J_\phi(r,t)H_z(r,t)[1 + a\sin\phi]^2 \\ &\quad \times [\cos\phi\vec{i}_x + \sin\phi\vec{i}_y]rdrd\phi \\ &= \vec{i}_y\int_{r=0}^{R} 2\pi a\mu J_\phi(r,t)H_z(r,t)rdr \\ &= -\frac{4\pi a\mu H_o^2}{R}\vec{i}_y\int_{r=0}^{R}\left[\sum_{n=1}^{\infty}\frac{J_1(\beta_n r/R)}{J_1(\beta_n)}e^{-\beta_n^2 t/\tau}\right] \\ &\quad \times \left[1 - 2\sum_{n=1}^{\infty}\frac{J_o(\beta_n r/R)}{\beta_n J_1(\beta_n)}e^{-\beta_n^2 t/\tau}\right]rdr. \end{aligned} \tag{91}$$

To evaluate (91) it is necessary to take a sufficient number of terms in the infinite series so that the remaining terms give

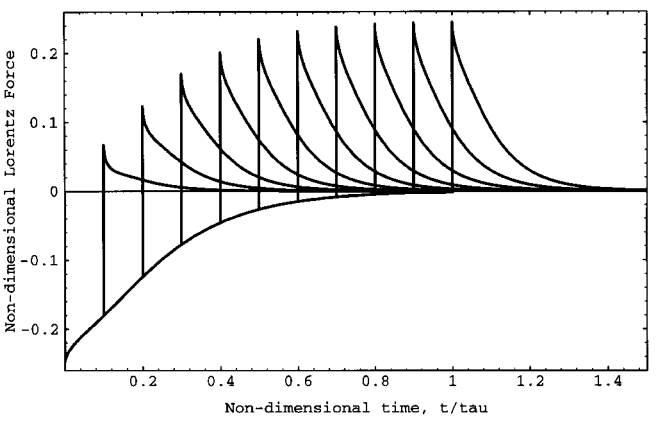

Fig. 14. The nondimensional Lorentz force, $f_{Ly}/(4\pi a\mu RH_o^2)$, versus t/τ using the first 20 terms in the series expressions for a step imposed axial magnetic field of time duration T. The Lorentz force for the step turn on transient in the time interval $0 < t < T$ of (91) is shown as the negative force. The Lorentz force during the turn off transient for $t > T$ is shown as the stepped positive forces for various values of T/τ and is obtained by substituting (96) and (97) into the top expression of (91).

a negligible contribution and then numerically integrate over r. The result is shown in Fig. 14 which plots the negative nondimensional Lorentz force of (91) versus nondimensional time using the first 20 terms in the series. The force becomes negligibly small for $t/\tau > 1$.

B. Turn-Off Transient

After a time T, the magnetic field is turned off. The initial and boundary conditions are then

$$H_z(r=R, t>T)=0$$
$$H_z(r,t=T)=H_o\left[1-2\sum_{n=1}^{\infty}\frac{J_o(\beta_n r/R)}{\beta_n J_1(\beta_n)}e^{-\beta_n^2 T/\tau}\right]. \tag{92}$$

For $t > T$ we thus take a solution of the form

$$H_z(r,t)=\hat{H}(r)e^{-\alpha(t-T)} \tag{93}$$

where the steady-state magnetic field ($t \to \infty$) is zero. The solution form is again given by (74) and (75)

$$H_z(r,t)=\sum_{n=1}^{\infty}A_n J_o(\beta_n r/R)e^{-\beta_n^2(t-T)/\tau}. \tag{94}$$

The amplitudes A_n are found using (92) and the orthogonal Bessel function relations of (79)

$$A_n=\frac{2}{R^2J_1^2(\beta_n)}\int_{r=0}^{R}H_z(r,t=T)J_o(\beta_n r/R)rdr$$
$$=\frac{2H_o[1-e^{-\beta_n^2 T/\tau}]}{\beta_n J_1(\beta_n)}. \tag{95}$$

The magnetic field and current density for $t > T$ are then

$$H_z(r,t)=2H_o\sum_{n=1}^{\infty}\frac{J_o(\beta_n r/R)[1-e^{-\beta_n^2 T/\tau}]}{\beta_n J_1(\beta_n)}e^{-\beta_n^2(t-T)/\tau} \tag{96}$$

$$J_\phi(r,t)=-\frac{\partial H_z}{\partial r}=\frac{2H_o}{R}\sum_{n=1}^{\infty}\frac{J_1(\beta_n r/R)[1-e^{-\beta_n^2 T/\tau}]}{J_1(\beta_n)}$$
$$\times e^{-\beta_n^2(t-T)/\tau}. \tag{97}$$

At $r/R = 1$, the magnetic field amplitude instantaneously drops from H_o to zero, causing a surface current in the opposite direction to the volume current flowing just before the magnetic field was turned off. This surface current then diffuses into the cylinder as a volume current, decreasing to near zero in a time of order τ.

The dissipated power and dissipated energy per unit length are then

$$P=\frac{8\pi H_o^2}{\sigma R^2}$$
$$\times\int_{r=0}^{R}\left[\sum_{n=1}^{\infty}\frac{J_1(\beta_n r/R)[1-e^{-\beta_n^2 T/\tau}]}{J_1(\beta_n)}e^{-\beta_n^2(t-T)/\tau}\right]^2 rdr$$
$$=\frac{4\pi H_o^2}{\sigma}\sum_{n=1}^{\infty}[1-e^{-\beta_n^2 T/\tau}]^2 e^{-2\beta_n^2(t-T)/\tau} \tag{98}$$

$$W=\int_{t=0}^{T}P(0<t<T)dt+\int_{t=T}^{\infty}P(t>T)dt$$
$$=2\pi\mu H_o^2R^2\sum_{n=1}^{\infty}\frac{[1-e^{-2\beta_n^2 T/\tau}]}{\beta_n^2}$$
$$+2\pi\mu H_o^2R^2\sum_{n=1}^{\infty}\frac{[1-e^{-\beta_n^2 T/\tau}]^2}{\beta_n^2}$$
$$=4\pi\mu H_o^2R^2\sum_{n=1}^{\infty}\frac{[1-e^{-\beta_n^2 T/\tau}]}{\beta_n^2} \tag{99}$$

This dissipated energy per unit length includes contributions from the turn on of the magnetic field at $t = 0$ and from the turn off of the magnetic field at time T. This dissipated energy per unit length is plotted versus T/τ in Fig. 15. Note that as T/τ becomes greater than one, the dissipated energy approaches $4\pi\mu H_o^2R^2(0.246)$, which is twice that computed for the stepped on field with $T \to \infty$. Thus for $T/\tau \gg 1$, as much energy is dissipated in turning on the magnetic field as for turning off the magnetic field.

The magnetization force is zero for $t > T$ as the magnetic field at the $r = R$ interface is zero. The Lorentz force for $t > T$ is shown as the stepped positive forces in Fig. 14 by substituting the magnetic field and current density of (96) and (97) into the top expression of (91).

VI. Step Change in Transverse Magnetic Field

A. General Solutions

A transverse x directed electric field is instantaneously stepped on at time $t = 0$ to an amplitude H_o. The solutions have a steady-state part and a transient part that dies out with time. The steady-state current density is zero so the general form for the current density is

$$J_z(r,\phi,t)=\hat{J}_z(r,\phi)e^{-\alpha t} \tag{100}$$

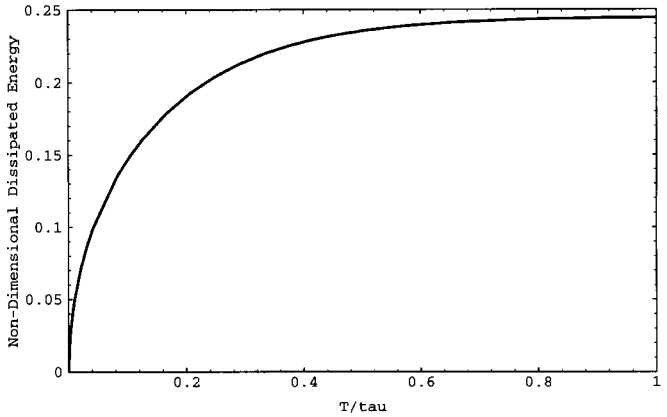

Fig. 15. Nondimensional dissipated energy $W/(4\pi\mu H_o^2 R^2)$ from (99) for a stepped on axial magnetic field of duration T as a function of T/τ.

which when substituted into (5) gives

$$\frac{1}{r}\frac{\partial}{\partial r}\left(r\frac{\partial \hat{J}_z}{\partial r}\right)+\frac{1}{r^2}\frac{\partial^2 \hat{J}_z}{\partial \phi^2}=-\alpha\mu\sigma\hat{J}_z. \tag{101}$$

The general product solution that is finite at $r=0$ is

$$\hat{J}_z(r,\phi)=J_m(\sqrt{\alpha\mu\sigma}r)[A_1\sin m\phi+A_2\cos m\phi]. \tag{102}$$

However, the uniform x directed magnetic field only excites the $m=1$ solution with $A_2=0$ so that the current density is of the form

$$J_z(r,\phi,t)=AJ_1(\sqrt{\alpha\mu\sigma}r)\sin\phi e^{-\alpha t}. \tag{103}$$

The magnetic-field solution in the cylinder for $r<R$ is obtained from Faraday's law of (1)

$$\frac{\partial \vec{H}}{\partial t}=-\frac{1}{\mu\sigma}\nabla\times\vec{J}=-\frac{1}{\mu\sigma}\left[\vec{i}_r\frac{1}{r}\frac{\partial J_z}{\partial\phi}-\vec{i}_\phi\frac{\partial J_z}{\partial r}\right] \tag{104}$$

while the magnetic field outside the cylinder for $r>R$ is obtained from a magnetic scalar potential or equivalently with a z directed magnetic vector potential, both obeying Laplace's equation. The radial and ϕ components of $\vec{H}$ for steady state and transients are thus of the form shown as follows and in (106) shown at the bottom of the page

$$H_r(r,\phi,t)=\begin{cases}\left[\frac{A}{\alpha\mu\sigma r}J_1(\sqrt{\alpha\mu\sigma}r)e^{-\alpha t}+\frac{2\mu_o H_o}{\mu+\mu_o}\right]\cos\phi & r<R\\ \left[\frac{Ce^{-\alpha t}}{r^2}+H_o\left[1+\frac{R^2(\mu-\mu_o)}{r^2(\mu+\mu_o)}\right]\right]\cos\phi & r>R\end{cases} \tag{105}$$

where it is necessary in time integrating (104) to include the steady-state solutions as constants of integration.

B. Boundary Conditions

The steady-state solutions already satisfy continuity of tangential $\vec{H}$ and normal $\vec{B}$ at $r=R$. The transient solutions must also obey these boundary conditions for which we obtain

$$\begin{aligned}H_\phi(r=R_+)=H_\phi(r=R_-)\Rightarrow\frac{C}{R^2}&=-\frac{A}{\alpha\mu\sigma}\Big[\sqrt{\alpha\mu\sigma}J_o(\sqrt{\alpha\mu\sigma}R)\\&\quad-\frac{1}{R}J_1(\sqrt{\alpha\mu\sigma}R)\Big]\\ \mu_o H_r(r=R_+)=\mu H_r(r=R_-)\Rightarrow\frac{\mu_o C}{R^2}&=\frac{A}{\alpha\sigma R}J_1(\sqrt{\alpha\mu\sigma}R)\end{aligned} \tag{107}$$

which for nonzero values of A and C require that

$$\mu_o\sqrt{\alpha\mu\sigma}RJ_o(\sqrt{\alpha\mu\sigma}R)+(\mu-\mu_o)J_1(\sqrt{\alpha\mu\sigma}R)=0. \tag{108}$$

This relation then determines allowed values of α which we denote as α_n with corresponding amplitudes A_n and C_n related through either of the relations in (107). Note that because

$$J_o(\beta)=\frac{dJ_1}{d\beta}+\frac{1}{\beta}J_1(\beta) \tag{109}$$

that (108) can be rewritten as

$$\mu J_1(\beta)+\mu_o\beta\frac{dJ_1}{d\beta}=0,\quad \beta=\sqrt{\alpha\mu\sigma}R \tag{110}$$

which is in the form of (84) with $a=\mu, b=\mu_o$, and $\nu=1$. If $\mu=\mu_o$, (108) shows that the β_n are the zeros of the zeroth order Bessel function listed in the left-most column of Table II while as μ/μ_o becomes very large, the β_n are the zeros of the first order Bessel function listed in the right-most column of Table II. Table II also lists the first 20 solutions to (108) for magnetic permeabilities that include materials in Table I. Note that as the β_n become large, the Bessel functions can be approximated as [2, Sec. 4.9]

$$\begin{aligned}\lim_{\beta\gg1}J_o(\beta)&\approx\sqrt{\frac{1}{\pi\beta}}(\sin\beta+\cos\beta)\\ J_1(\beta)&\approx\sqrt{\frac{1}{\pi\beta}}(\sin\beta-\cos\beta)\end{aligned} \tag{111}$$

which when substituted into (108) gives

$$\lim_{\beta\gg1}\tan\beta\approx\frac{\mu-\mu_o(1+\beta)}{\mu-\mu_o(1-\beta)}. \tag{112}$$

For $\mu=\mu_o$, this gives solution $\tan\beta\approx-1$ so that $\beta_n\approx(n-0.25)\pi$. For $\mu\gg\mu_o$, the solution is $\tan\beta\approx1$ and $\beta\approx(n+0.25)\pi$.

$$H_\phi(r,\phi,t)=\begin{cases}\left[-\frac{A}{\alpha\mu\sigma}\left[\sqrt{\alpha\mu\sigma}J_o(\sqrt{\alpha\mu\sigma}r)-\frac{1}{r}J_1(\sqrt{\alpha\mu\sigma}r)\right]e^{-\alpha t}-\frac{2\mu_o H_o}{\mu+\mu_o}\right]\sin\phi, & r<R\\ \left[\frac{Ce^{-\alpha t}}{r^2}-H_o\left[1-\frac{R^2(\mu-\mu_o)}{r^2(\mu+\mu_o)}\right]\right]\sin\phi, & r>R\end{cases} \tag{106}$$

If the infinite number of solutions to (110) are denoted as β_n, then the Bessel function orthogonality relation of (83) is

$$\int_0^1 \left(\frac{r}{R}\right) J_1(\beta_n r/R) J_1(\beta_m r/R) \left(\frac{dr}{R}\right) = \begin{cases} 0 & m \neq n \\ \frac{1}{2\beta_n^2}\left[\frac{\mu^2}{\mu_o^2} + \beta_n^2 - 1\right] J_1^2(\beta_n), & m = n. \end{cases} \quad (113)$$

The general form of solution for the current density of (102) is

$$J_z(r,\phi,t) = \sum_{n=1}^{\infty} A_n J_1(\beta_n r/R) e^{-\beta_n^2 t/\tau} \sin\phi \quad (114)$$

where $\tau = \sigma\mu R^2$ is a representative magnetic diffusion time. The coefficients A_n can be obtained using the orthogonality condition of (113) with the initial condition that at $t = 0$, all the current flows as a surface current at $r = R$ and is thus a spatial impulse at $r = R$

$$J_z(r,\phi,t=0) = -2H_o \sin\phi \delta(r-R) = \sum_{n=1}^{\infty} A_n J_1(\beta_n r/R) \sin\phi. \quad (115)$$

Multiplying both sides of (115) by $(r/R)J_1(\beta_m r/R)$ and integrating over $d(r/R)$ lets us solve for A_n

$$\int_0^1 -\frac{2H_o r}{R} J_1(\beta_m r/R)\delta(r-R)\frac{dr}{R} = -\frac{2H_o J_1(\beta_m)}{R} = \frac{A_m}{2\beta_m^2}\left[\frac{\mu^2}{\mu_o^2} + \beta_m^2 - 1\right] J_1^2(\beta_m) \quad (116)$$

as

$$A_n = -\frac{4\beta_n^2 H_o}{R\left[\frac{\mu^2}{\mu_o^2} + \beta_n^2 - 1\right] J_1(\beta_n)}. \quad (117)$$

C. Magnetic-Field Lines

For transient solutions, the magnetic-field lines are also the lines of constant magnetic potential defined in (57). The vector potential is then obtained from (105)–(106) as shown in (118) at the bottom of the page. Figs. 16 and 17 plot the magnetic-field lines as a function of time for $\mu/\mu_o = 1$ and 10 using the first 20 terms in the series expressions. At $t = 0$, the magnetic field is excluded from the cylinder. As t increases the magnetic field diffuses into the cylinder approaching the steady state for $t/\tau > 0.5$. As μ/μ_o becomes large, it requires many more terms in the Fourier series for accurate solutions near $t = 0$.

D. Dissipated Power Per Unit Length

To summarize the procedure, β_n must be found by numerically solving (108). Then the A_n are found from (117) and the current density is found from (114). The dissipated power per unit length is given by

$$\begin{aligned} P &= \int_{r=0}^{R}\int_{\phi=0}^{2\pi} \frac{J_z^2}{\sigma} r dr d\phi \\ &= \frac{1}{\sigma}\int_{r=0}^{R}\int_{\phi=0}^{2\pi}\left[\sum_{n=1}^{\infty} A_n J_1(\beta_n r/R) e^{-\beta_n^2 t/\tau}\right]^2 \sin^2\phi r dr d\phi \\ &= \frac{\pi}{\sigma}\int_{r=0}^{R}\left[\sum_{n=1}^{\infty} A_n J_1(\beta_n r/R) e^{-\beta_n^2 t/\tau}\right]^2 r dr \\ &= \frac{\pi R^2}{2\sigma}\sum_{n=1}^{\infty}\frac{A_n^2}{\beta_n^2}\left[\left(\frac{\mu}{\mu_o}\right)^2 + \beta_n^2 - 1\right] J_1^2(\beta_n) e^{-2\beta_n^2 t/\tau} \\ &= \frac{8\pi H_o^2}{\sigma}\sum_{n=1}^{\infty}\frac{\beta_n^2 e^{-2\beta_n^2 t/\tau}}{\left[\left(\frac{\mu}{\mu_o}\right)^2 + \beta_n^2 - 1\right]} \end{aligned} \quad (119)$$

where we used (113) to perform the integrations. The total dissipated energy per unit length is then

$$W = \int_0^{\infty} P dt = 4\pi\mu H_o^2 R^2 \sum_{n=1}^{\infty}\frac{1}{\left[\left(\frac{\mu}{\mu_o}\right)^2 + \beta_n^2 - 1\right]} \quad (120)$$

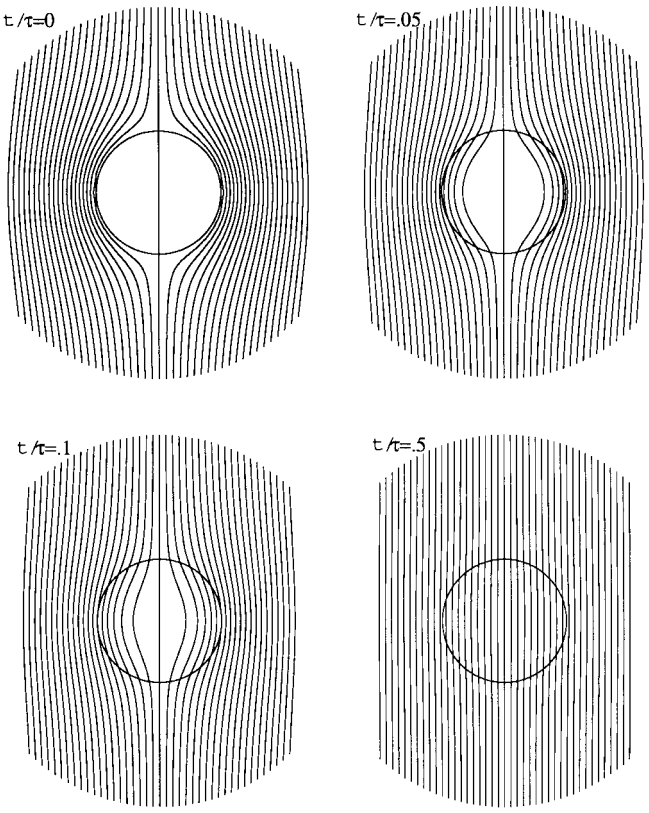

Fig. 16. Magnetic-field lines of (118) using the first 20 terms in the series for various times after a transverse magnetic field is stepped on at $t = 0$ for $\mu/\mu_o = 1$.

$$A_z(r,\phi,t) = \begin{cases} \sum_{n=1}^{\infty} \mu\left[\frac{A_n R^2}{\beta_n^2} J_1(\beta_n r/R) e^{-\beta_n^2 t/\tau} + \frac{2\mu_o H_o r}{\mu+\mu_o}\right] \sin\phi, & r < R \\ \sum_{n=1}^{\infty} \mu_o\left[\frac{C_n e^{-\beta_n^2 t/\tau}}{r} + H_o\left[r + \frac{R^2(\mu-\mu_o)}{r(\mu+\mu_o)}\right]\right] \sin\phi, & r > R \end{cases} \quad (118)$$

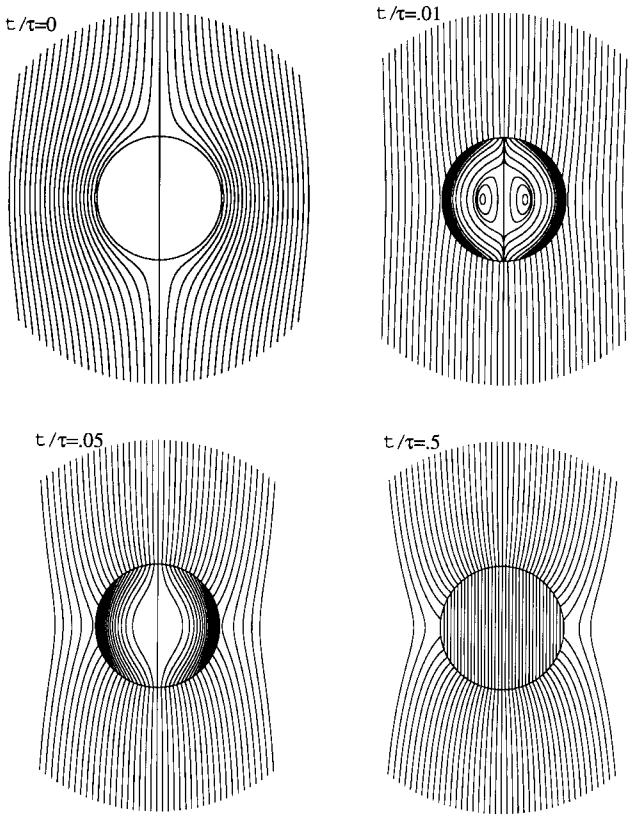

Fig. 17. Magnetic-field lines of (118) using the first 20 terms in the series for various times after a transverse magnetic field is stepped on at $t = 0$ for $\mu/\mu_o = 10$.

TABLE III
NONDIMENSIONAL DISSIPATED ENERGY PER UNIT LENGTH FROM (120) DUE TO A STEPPED ON TRANSVERSE MAGNETIC FIELD, $W/(4\pi\mu H_o^2 R^2)$, FOR MAGNETIC PERMEABILITY VALUES IN TABLE I, USING THE β_n VALUES IN TABLE II

Material	μ/μ_o	$W/(4\pi\mu H_o^2 R^2)$
Aluminum, copper, and Stainless Steel	1	0.245
13 Mn Steel	1.01	0.244
	10	0.040
Grade 50 and 60 Rebar Steel	3800	1.385×10^{-6}
Mild Steel	5000	8.000×10^{-7}

where the β_n are given in Table II for μ/μ_o values that include materials in Table I. Table IIIuses Table II values for β_n to compute (120) for various values of μ/μ_o.

E. Magnetization Force Per Unit Length

At the interface we have from (105) and (106)

$$H_\phi(r=R,\phi,t) = \left[\sum_{n=1}^{\infty}\frac{C_n}{R^2}e^{-\beta_n^2 t/\tau} - \frac{2\mu_o H_o}{(\mu+\mu_o)}\right]\sin\phi = H_\phi(t)\sin\phi$$
$$B_r(r=R,\phi,t) = \left[\sum_{n=1}^{\infty}\frac{\mu_o C_n}{R^2}e^{-\beta_n^2 t/\tau} + \frac{2\mu\mu_o H_o}{(\mu+\mu_o)}\right]\cos\phi = B_r(t)\cos\phi \quad (121)$$

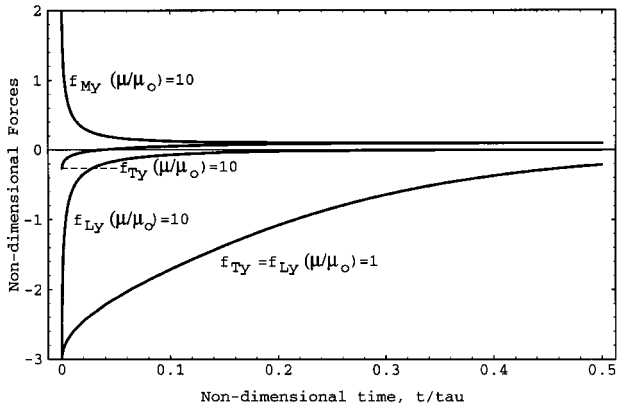

Fig. 18. Nondimensional forces of (124), $f_{My}/(\pi Ra\mu H_o^2)$, (125), $f_{Ly}/(\pi Ra\mu H_o^2)$, and their sum, $f_T/(\pi Ra\mu H_o^2) = (f_{Ly} + f_{My})/(\pi Ra\mu H_o^2)$ versus nondimensional time t/τ for values of $\mu/\mu_o = 1$ and 10. For $\mu/\mu_o = 1$, $f_{My} = 0$.

where we separate out the time and ϕ dependences and from (107)

$$C_n = \frac{\mu A_n R^3 J_1(\beta_n)}{\mu_o \beta_n^2}. \quad (122)$$

From (13) and the assumed weak gradient field of (14), the magnetization force per unit length is

$$\vec{f}_M = \frac{R}{2}\int_{\phi=0}^{2\pi}\left[(\mu-\mu_o)H_\phi^2(t)\sin^2\phi + \left(\frac{1}{\mu_o}-\frac{1}{\mu}\right)B_r^2(t)\cos^2\phi\right] \times [1+a\sin\phi]^2[\vec{i}_x\cos\phi + \vec{i}_y\sin\phi]d\phi. \quad (123)$$

Performing the ϕ integration gives

$$f_{My} = \frac{\pi Ra}{4}\left[3(\mu-\mu_o)H_\phi^2(t) + \left(\frac{1}{\mu_o}-\frac{1}{\mu}\right)B_r^2(t)\right]. \quad (124)$$

At $t = 0$, $H_\phi(t=0) = -2H_o$ and $B_r(t=0) = 0$, so that $f_{My}(t=0) = 3\pi Ra(\mu-\mu_o)H_o^2$. As $t\to\infty$, $f_{My}(t\to\infty) = \frac{\pi Ra H_o^2\mu_o^2(\mu-\mu_o)(3+\mu/\mu_o)}{(\mu+\mu_o)^2}$. The magnetization force of (124) versus nondimensional time is plotted in Fig. 18 as a positive force for $\mu/\mu_o = 10$. For $\mu/\mu_o = 1, f_{My} = 0$.

F. Lorentz Force Per Unit Length

From (60), the Lorentz force per unit length is

$$\vec{f}_L = \int_{r=0}^{R}\int_{\phi=0}^{2\pi} J_z(r,t)\sin\phi \times [B_r(r,t)\cos\phi(-\sin\phi\vec{i}_x + \cos\phi\vec{i}_y) - \mu H_\phi(r,t)\sin\phi(\cos\phi\vec{i}_x + \sin\phi\vec{i}_y)] \times [1+a\sin\phi]^2 r\,dr\,d\phi = \frac{\pi a}{2}\vec{i}_y\int_{r=0}^{R} J_z(r,t)[B_r(r,t) - 3\mu H_\phi(r,t)]r\,dr \quad (125)$$

which is evaluated by numerical integration and is plotted as a negative force in Fig. 18 for $\mu/\mu_o = 1$ and 10. At $t = 0$, the Lorentz force per unit length is $f_{Ly} = -3\pi Ra\mu H_o^2$ which decreases to zero as time increases. The total nondimensional

force per unit length, given by the sum of (124) and (125), is also plotted in Fig. 18 and for $\mu/\mu_o > 1$ is negative for early time due to the Lorentz force, passes through zero, and is then positive for longer time due to the magnetization force. At $t = 0$ the total force is $f_{Ly} + f_{My} = -3\pi Ra\mu_o H_o^2$.

ACKNOWLEDGMENT

The author gratefully acknowledges stimulating discussions with R. D. Thornton. Undergraduate students A. D. Lobban, D. J. Lisk, R. Karmacharya, and E. Warlick assisted in preparing some of the plots as part of the Massachusetts Institute of Technology Undergraduate Research Opportunities Program (UROP). All the plots were prepared using Mathematica [7].

REFERENCES

[1] M. Zahn, *Electromagnetic Field Theory: A Problem Solving Approach*. Melbourne, FL: Krieger, 1987.
[2] F. B. Hildebrand, *Advanced Calculus for Applications*. Englewood Cliffs, NJ: Prentice-Hall, 1965.
[3] N. W. McLachlan, *Bessel Functions for Engineers*. London, UK: Clarendon Press, 1961.
[4] M. P. Perry, *Low Frequency Electromagnetic Design*. New York: Marcel Dekker, 1985.
[5] W. R. Smythe, *Static and Dynamic Electricity*. New York: McGraw-Hill, 1968.
[6] M. Abramowitz and I. A. Stegun, Eds., *Handbook of Mathematical Functions* (Applied Mathematics Series 55). Washington, DC: NBS, 1968.
[7] S. Wolfram, *Mathematica, A System for Doing Mathematics by Computer*. Redwood City, CA: Addison-Wesley, 1991.